Design and Evaluation of Nonlinear Verification Device for Nonlinear Vector Network Analyzers

Mohammad Rajabi, *Student Member, IEEE,* David A. Humphreys, *Senior Member, IEEE,* Gustavo Avolio, *Member, IEEE,* Paweł Barmuta, *Student Member, IEEE,* Konstanty R. Łukasik, *Student Member, IEEE,* Troels S. Nielsen, *Member, IEEE,* and Dominique M. M.-P. Schreurs, *Fellow, IEEE*

***Abstract*—A simple diode-based Nonlinear Verification Device (NVD) design for Nonlinear Vector Network Analyzers is presented together with an improved Figure of Merit (FOM) parameter that is insensitive to impedance match and isolates variation of the device's nonlinear parameters. The stability over 84 hours and load-pull performance of this new design have been evaluated.**

***Index Terms*—Nonlinear circuits, instrumentation and measurement, measurement uncertainty, microwave integrated circuits, nonlinear network analysis, semiconductor diodes.**

I. Introduction

RF circuit design has evolved to accommodate the twin demands of higher Peak-to-Average-Power-Ratio (PAPR) designs and higher power efficiency, driven by RF communications. Measurement and testing is an important part of the process and until recently, the Vector Network Analyzer (VNA) has been the test instrument of choice. Driven by the development of high-efficiency power amplifiers that are suited to the emerging complex communication waveforms, nonlinear Vector Network Analyzers (NVNA) have moved from niche to mainstream over the past ten years [1], [2].

Over the last thirty years progress has been made to improve the traceability of VNA measurements and to explore the stability performance of calibration aids such as e-cal systems. Even though VNA receivers measure the wave quantities, only the ratios of these quantities are required to fully describe linear Devices Under Test (DUT). Therefore, the knowledge of neither the absolute values of the waves nor their phase relationships over frequency is needed. This allows to use linear components, such as shorts, opens, thru lines, etc., as calibration standards. Such standards are easily traceable to measurements of their physical dimensions and material properties. Contrary to VNA measurements, in NVNA measurements the information about the absolute amplitude and phase is crucial for the correct DUT description. To support this, the NVNA is calibrated so that it is traceable to absolute voltage, defined in terms of the transmission line characteristic impedance and the RF power. Generated waveforms from a nonlinear device contain both fundamental and harmonics. Therefore, a phase calibration is required to identify phase-relationships between signal elements at multiple frequencies whereas an RF power calibration is needed to measure signal absolute power. Standards employed in phase and power calibration are traceable to RF power and electro-optic measurements within a National Metrology Institute (NMI). Therefore, NVNA calibration has more parameters influencing the uncertainty of NVNA measurement [3].

Quality verification of a VNA calibration can be achieved using an artifact, such as an offset short or an air-line [4]. It is more difficult to properly validate the calibration quality of an NVNA as this requires a stable active device with a traceable and reproducible response. Several Nonlinear Verification Device (NVD) approaches have been reported [5]–[7] and a Figure of Merit (FOM) (4) was proposed as part of the IMS 2012 student competition. All of the designs were excited at 2 GHz and the FOM were measured based on the first five harmonics. The application is intended for one fundamental frequency. In fact, by a quick verification by the user, a potential structural calibration problem may be revealed, in terms of wrongly executing the calibration procedure by an inexperienced user. For such application, the fundamental frequency can be a general value, such as in this work.

Some of these nonlinear verification device designs [5], [6] as shown in Fig. 1a are quite complicated. An example shown in of Fig. 1a uses a Class-C amplifier, isolated from feedback using a linear amplifier [5]. The reported FOM evaluated by using five loads ($|\Gamma| < 0.2$) is 1.5%. In contrast to using amplifiers to generate harmonics or to make a buffer component, we present a novel design, based on a four-diode circuit. It is simpler and less expensive than the design in Fig. 1a. Moreover, one of the potential advantages of a diode over a cascade of amplifiers and attenuators is traceability. As in the case of the passive calibration standards [8], one may also try to establish traceability path to the physical dimensions of the circuit and the corresponding material properties . As the diode can be described by a relatively simple behavioural model

Manuscript received April 6, 2017. This work has been supported by the EMRP joint research project "SIB62 HF Circuits". The EMRP is jointly funded by the EMRP participating countries within EURAMET and the European Union. We extend the acknowledgment to the financial support by FWO and Hercules.

M. Rajabi, G Avolio, P. Barmuta, K. R. Łukasik and D. M. M.-P. Schreurs are with the Department of Electrical Engineering, KU Leuven, 3003 Leuven, Belgium (e-mail: mohammad.rajabi@kuleuven.be).

P. Barmuta and K. R. Łukasik are with the Faculty of Electronic and Information Technology, Warsaw University of Technology, 00-665 Warsaw, Poland.

D. A. Humphreys is with the National Physical Laboratory, Teddington TW11 0LW, United Kingdom (e-mail: david.humphreys@npl.co.uk), and University of Bristol, Room 5.17, Merchant Venturturers Building, Woodland Road, Bristol, United Kingdom.

T. S. Nielsen is with Keysight Technologies, Alfred Nobels Vej 21D, 9220 Aalborg East, Denmark

Color versions of one or more of the figures in this paper are available online at http://ieeexplore.ieee.org.

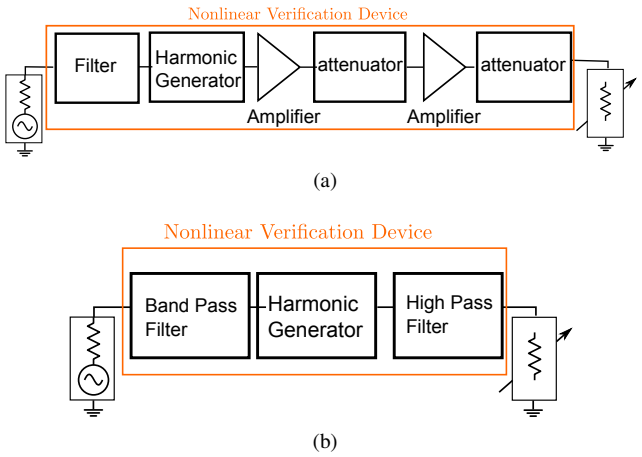

Figure 1. Approaches to design a Nonlinear Verification Device. (a) Existing designs [5], [6]; (b) and the proposed design.

and the embedding network is passive, calculating the overall model and uncertainties is straightforward when compared with the earlier designs. Earlier designs use a cascade of amplifiers and attenuators that results in a very complex circuit with a huge number of potential error sources in uncertainty analysis.

Besides using an NVD for calibration-comparison, another approach was proposed in [9], that, instead of using a single NVD to evaluate an NVNA calibration, a complete and traceable calibration kit (consisting of additional scattering-parameter calibration artifacts, phase reference, and power meter) is used to assess the accuracy of a user's working calibration. This approach is used in [10] as part of the IMS 2015 student competition.

The earlier papers [7], [11] describing the diode-based nonlinear verification device (NVD) have been extended to explain the rationale for the revised FOM and this is demonstrated using the second NVD design. Also, this second NVD design is described in detail.

This paper is organized as follows: in Section II we outline the existing evaluation criterion and propose a revised criterion that isolates the sensitivity of the nonlinear component to output reflection coefficients; in Section III, we describe the adopted design, and in Section IV, measurement results are presented. Finally, conclusions and future activity are discussed in Section V.

II. Nonlinear Verification Device Attributes and Evaluation Criteria

A. Nonlinear verification device

The NVD aims to give identical harmonic-performance irrespective of the load match. The NVNA match will depend on the instrument's intrinsic properties and the cabling. A key attribute of the evaluation criterion is that it must uniquely identify the sensitivity of the nonlinear element to feedback from the NVNA ports. This result must not be influenced by the NVNA port match. The main issue arises from the phenomenon that any nonlinear device behavior depends on DC bias and incident waves on its both ports. For a given nonlinear block (device) shown in Fig. 2a, we can determine a complex function H that maps all of the input incident waves a_{1NL,mf_0} and a_{2NL,nf_0} with the output scattered waves b_{2NL,kf_0}, whereby m, n and k range from one to the highest harmonic index. This is mathematically expressed as [12]

$$b_{2NL,kf_0} = H(DC, a_{1NL,f_0}, a_{1NL,2f_0}, \ldots , a_{2NL,f_0}, a_{2NL,2f_0}, \ldots). \quad (1)$$

NVD is made of two passive blocks and one nonlinear block shown in Fig. 2b. b_2 coming out of the input of passive block 2 and $a_{2,NL}$ going in the output of nonlinear block are identical, b_{2NL} and a_2 are identical as well.

Each NVNA presents different impedances to NVD at the fundamental and harmonic frequencies. The reflected wave from the load, which is a_3 in Fig. 2b, passing the passive block becomes b_2. This variation of b_2 changes the response of function H (1) that results in another value of a_2. The design of a passive block 2 allows to reduce this variation. Therefore, the load dependency of nonlinear devices is one of the major attributes that results in failure of any proposed NVD design or round-robin device [13] until one does consider the impedance mismatch influence.

Stability and reproducibility are other essential criteria for any verification device. Keeping the design simple reduces the number of potential error sources [14]. Aging might as well influence the NVD characteristics [15].

Furthermore, an Electronic Calibration Unit (ECU) can be used as a linear verification device [16]. In principle, if all mentioned requirements are met for the NVD, then the NVD could be included in the ECU. As a result, the ECU could be used for verification of both linear and absolute calibration of an NVNA.

B. Verification criteria

The FOM to evaluate the influence of the impedance mismatch on the response of the NVD used in earlier work, [5]–[7], is based on the variation of the normalized phase value of $\widetilde{b_3}$ (scattered wave at the output of the NVD that is measured by NVNA output port), where

$$\widetilde{b_3}(nf_0, \Gamma_{m,nf_0}) = \left(\frac{a_1^*}{|a_1|}\right)^n b_3(nf_0, \Gamma_{m,nf_0}) \quad (2)$$

and n is the harmonic frequency of f_0, where (Γ_{m,nf_0}) is the reflection coefficient corresponding to the mth load at frequency nf_0, with a mean value $\bar{b_3}(nf_0)$ at each frequency for M loads:

$$\bar{b_3}(nf_0) = \frac{1}{M}\sum_{m=1}^{M} \widetilde{b_3}(nf_0, \Gamma_{m,nf_0}) \quad (3)$$

giving a FOM

$$FOM = \sqrt{\frac{1}{NM}\sum_{n=1}^{N}\sum_{m=1}^{M} \frac{\left|\widetilde{b_3}(nf_0, \Gamma_{m,nf_0}) - \bar{b_3}(nf_0)\right|^2}{|\bar{b_3}(nf_0)|^2}}. \quad (4)$$

Another FOM can also be defined at nth harmonic (FOM_{nf0}) as follows:

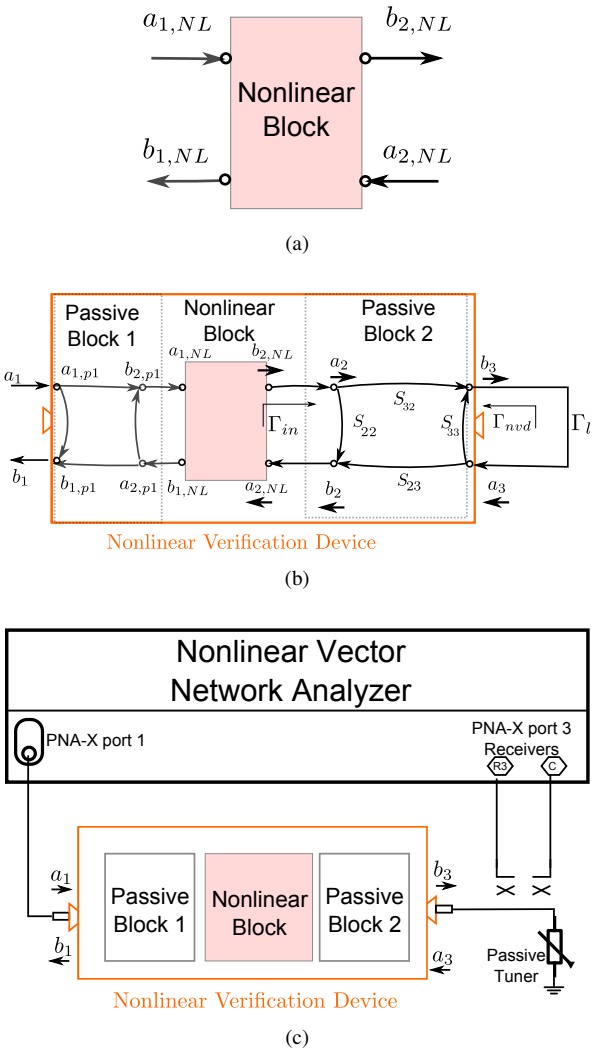

Figure 2. (a) The nonlinear block and (b) the flow graph of the NVD design and (c) measurement set-up. In (c), a_1, a_3, b_1 and b_3 are measured by NVNA.

$$FOM_{nf_0} = \sqrt{\frac{1}{M}\sum_{m=1}^{M}\frac{\left|\widetilde{b_3}(nf_0,\Gamma_{m,nf_0}) - \bar{b_3}(nf_0)\right|^2}{|\bar{b_3}(nf_0)|^2}} \quad (5)$$

The earlier figures of merit (4) and (5) are sensitive to both linear impedance mismatch and to sensitivity of the nonlinear element to feedback that we explain more later. We have therefore altered the figure of merit to reduce its sensitivity to load match. We propose a revised Figure of Merit (revised FOM) that is insensitive to NVNA impedance mismatch. The values of $\widetilde{b_3}$ are corrected for load mismatch using [17], [18]

$$\widetilde{b_3'}(nf_0,\Gamma_{m,nf_0}) = \left(\frac{a_1^*}{|a_1|}\right)^n b_3(nf_0,\Gamma_{m,nf_0})\,(1-\Gamma_{m,nf_0}\hat{\Gamma}_{nvd,nf_0}) \quad (6)$$

where the $a_1{}^*$ operator is complex conjugate of a_1 and $\hat{\Gamma}_{nvd,nf_0}$ is the NVD's estimated output impedance at nf_0 frequency. This transformation is based on the linear system theory to perform the mismatch correction under the condition that Γ_{nvd,nf_0} does not change, if Γ_{m,nf_0} is changing. The important point is that if the feedback ($a_{2,NL}$ in (1) and in Fig. 2b) does not affect the large-signal operating point, then $\widetilde{b_3'}(nf_0,\Gamma_{m,nf_0})$ loses its dependence on the match terms and becomes $\widetilde{b_3'}(nf_0)$. This allows solving for b_3 and Γ_{nvd} using least squares methods

$$\begin{bmatrix} \widetilde{b_3}(nf_0,\Gamma_{1,nf_0}) \\ \cdot \\ \cdot \\ \widetilde{b_3}(nf_0,\Gamma_{M,nf_0}) \end{bmatrix} = \begin{bmatrix} 1 & \widetilde{a_3}(nf_0,\Gamma_{1,nf_0}) \\ \cdot & \cdot \\ \cdot & \cdot \\ 1 & \widetilde{a_3}(nf_0,\Gamma_{M,nf_0}) \end{bmatrix} \begin{bmatrix} \hat{b_3}_{nvd,nf_0} \\ \hat{\Gamma}_{nvd,nf_0} \end{bmatrix} \quad (7)$$

The resulting values for $\hat{\Gamma}_{nvd,nf_0}$ can be used to determine $\widetilde{b_3'}(nf_0,\Gamma_{m,nf_0})$. Using $\widetilde{b_3'}(nf_0,\Gamma_{m,nf_0})$ in (4) and (5) gives the revised FOM and FOM_{nf0}, respectively.

The main disadvantage of FOM is that the load variation distribution is included in FOM. Assume there is a linear passive circuit instead of the NVD in Fig. 2c. The loadpull measurement is performed and different b_3s at the output are measured each time. The calculated FOM_{1f0} based on the linear DUT does not represent the properties (constant s-parameters) of the linear passive circuit that is load-independent. The FOM_{1f0} just represents a value that relates to load variation distribution. Using the revised FOM_{1f0} results in zero that means that the linear passive circuit is load-independent. Therefore, using the FOM instead of the revised FOM will lead in misrepresentation of the DUT's characteristics. The revised FOM excludes the contribution of the load variation distribution from the FOM.

Moreover, this type of FOM (4) represents a Coefficient of Variation (CV) of b_3, that will result in a biased estimation when the number of considered loads is small. Therefore, high number of loads is essential. Since we want to make a comparison with other designs such as [5] and [6], FOM_{nf0}, FOM, revised FOM_{nf0}, and revised FOM are reported in Section IV.

C. Verification of NVNA calibration

In the previous subsection, we proposed the revised FOM to evaluate any NVD's sensitivity to different loads and compare to other NVDs. In this subsection, we explain the possible approaches to verify a user's calibration by using our proposed NVD that has different topology and technology than the Harmonic Phase Reference (HPR) that is used in phase calibration step. After calibration, a user can measure our proposed NVD's $\widetilde{b_3}$ and $\widetilde{a_3}$. Then:

- The user can use a traceable model provided by a metrology institution. The model is a function of Γ_l. The user can compare the $b_{3\,measured}$ to the model's $b_{3\,reference}(\Gamma_l)$ to evaluate the calibration
- The user applies a mismatch correction to get $b_{3\,NVD\,m}$ in order to predict the b_3 under the condition that the load was 50 Ohm

$$b_{3\,NVD\,m} = \widetilde{b_3} - \widetilde{a_3}\Gamma_{NVD\,ref}$$

where $\Gamma_{NVD_{ref}}$ is a fully characterized reflection coefficient of the NVD. Therefore, the NVD should be characterized and modeled by another trusted measurement, such as a traceable NVNA setup. By comparing

the $b_{3\,NVD\,m}$ to the trusted $b_{3\,NVD\,reference}$ provided by a metrology lab, it is possible to verify the user's calibration. This method is bandwidth limited due to its design method.

Another approach is to verify the calibration by using our proposed NVD instead of the expensive HPR that was used in [10].

III. Nonlinear Verification Device Design

Fig. 3 shows the schematic of the proposed NVD. The input passive block is a coupled lines-based filter to pass the fundamental frequency, and to protect the nonlinear device from feedback caused by arbitrary harmonic source match. This is an improvement over the original design [7] in which an inductor was used as a filter element.

The non-linear block takes care of generating the fundamental and harmonic frequencies spectrum. One of the main objectives is to have an NVD based on diodes, and not amplifiers, to reduce the traceability procedure's complexity of the device to EOS compared to earlier prototypes [5], [6], [19].

The non-linear block is an IC that contains four medium barrier diodes in limiter configuration (Fig. 3). The Medium Barrier Diodes can be readily integrated into a microwave design, and are capable of handling high drive levels without degrading frequency performance [20]. The objective of the passive circuit following the nonlinear block is to reduce the sensitivity of the verification device to output mismatches.

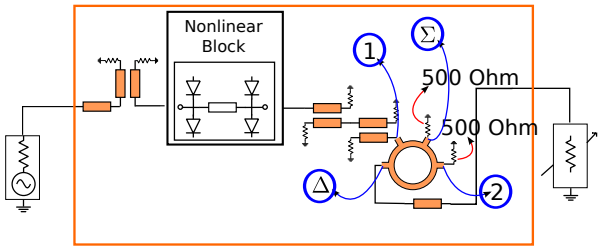

Figure 3. Simplified block diagram of the proposed NVD consisting of a nonlinear block to generate a train of harmonics, and an input passive block to pass the fundamental frequency, and an output passive block to improve the performance of the total circuit with respect to output mismatch.

The output passive structure consists of two cascaded coupled lines and a rat-race coupler. By using two-stage coupled lines and using the isolated ports of the coupled lines, an isolator and a high-pass filter function are achieved. Another coupled-line coupler is not used at the output because it would provide too much attenuation. Instead, a rat-race is used to increase the performance of the NVD compared to our previous design in [7] based on evaluating different structures and their ports by simulating the FOM [7].

The structure of rat-race coupler is shown in Fig. 3. By connecting the load to the Δ-port and by using resistors ($\neq 50\,\Omega$) connected to the Σ-port and Port 2 of the rat-race shown in Fig. 3, the FOM decreases for the odd harmonics when Γ_l is larger than the set criteria, e.g., $0.1 < |\Gamma_l| < 0.5$.

By connecting the nonlinear block to the passive circuit, the harmonics have similar power level as the fundamental

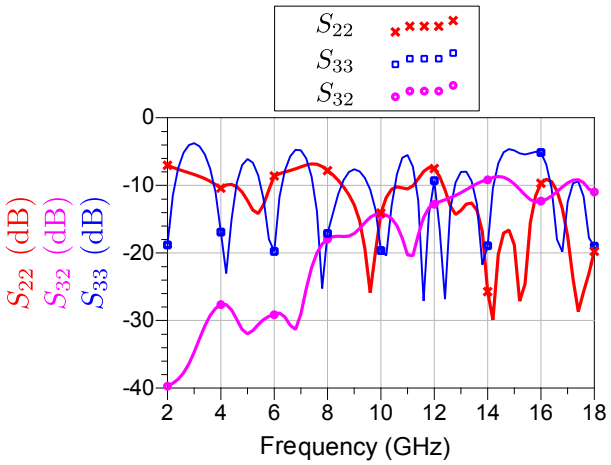

Figure 4. Simulated S-parameters of the stand-alone output passive block shown in Fig. 2b. The symbols are shown only at the fundamental and harmonic frequencies, corresponding to the designed NVD.

but with different phases, which results in lower PAPR unlike the design in [21] that is based on "pulse generation with Step Recovery Diode" to generate harmonics. Having a low PAPR signal at the output of the NVD is an advantage to use the NVD for verifying an oscilloscope calibration [22].

The output passive block is essential to isolate the nonlinear block from the load. The simulated S-parameters of the stand-alone output passive block are shown in Fig. 4. The fundamental frequency signal that has the highest power at the nonlinear block's output sees a large mismatch due to the highpass filtering behavior of the output passive block. Thus, the reflected wave will drive the diodes into more nonlinear operation and the resulting harmonics will be stronger.

This high reflection which exists inside the circuit itself will help to reduce changes' rate of the behavior of nonlinear block. As shown in Fig. 2b, the reflected waves returning to the nonlinear block at its output have following sources: 1) the ones reflected back from the passive circuit inside the device itself; and 2) the ones that are reflected back from the load (measurement instrument port). The nonlinear block sees Γ_{in} that has a part related to S_{22} (a load-independent parameter) and a part that depends on Γ_l (a load-dependent parameter), which is linked to the measurement instrument, and that can vary from instrument to instrument. Reflection coefficient Γ_{in} can be written as function of the load (Γ_l):

$$\Gamma_{in} = b_2/a_2 \tag{8}$$

$$\Gamma_{in} = S_{22} + \frac{S_{32}S_{23}\Gamma_l}{1 - S_{33}\Gamma_l} \tag{9}$$

Since we are using a reciprocal passive circuit after the nonlinear block (Fig. 2b), S_{23} is the same as S_{32}. Therefore, (8) and (9) become

$$b_2 = \underbrace{a_2 S_{22}}_{\text{Load}-\text{independent}} + \underbrace{\frac{a_2 (S_{23})^2}{1 - S_{33}\Gamma_l}\Gamma_l}_{\text{Load}-\text{dependent}} \tag{10}$$

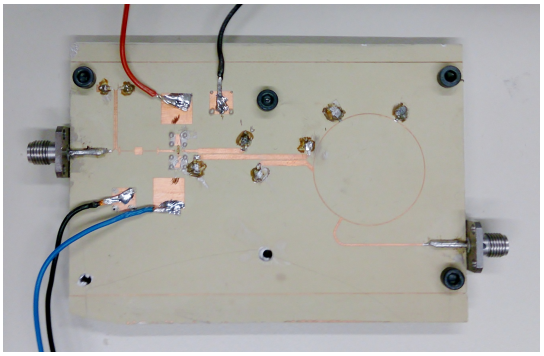

Figure 5. Picture of the realized Nonlinear Verification Device (NVD)

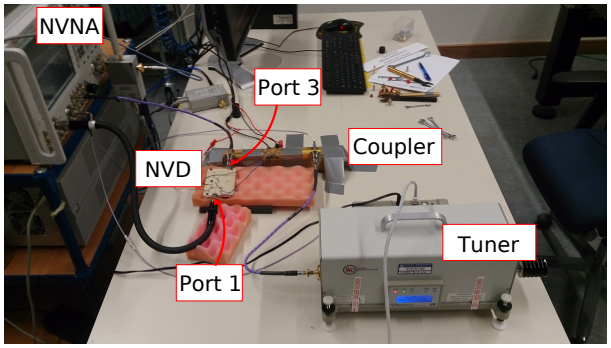

Figure 6. Measurement setup to change the load after calibration from $50\,\Omega$ to any desired value by using an automated passive dual-frequency tuner.

The first part is load-independent but the second part is load-dependent. The nonlinear block's behavior will be less affected by load variation, if the load-independent part of the wave is stronger than the load-dependent part of the wave. This conclusion was verified in the Monte Carlo analysis which we performed to determine the most suitable passive circuit to make the behavior of the nonlinear block less sensitive to mismatches [7]. The usage of matched attenuators showed worse results than, the considered passive circuits, that in addition to high attenuation, showed also high mismatch to the nonlinear block.

IV. Experimental Results and Discussion

Load Impedance Mismatch Evaluation

The realized circuit is shown in Fig. 5. The two-port measurement of the nonlinear verification device was done by an NVNA. The Intermediate Frequency Band Width (IFBW) in our NVNA settings is 3 Hz to decrease the noise floor, even less than the default setting. The default IFBW is 10 Hz that results in noise floor as -119 dBm (1 GHz to 10 GHz), -121 dBm (10 GHz to 16 GHz), and -122 dBm (16 GHz to 26.5 GHz). We used the measurement setup that is shown in Fig. 2c and Fig. 6. This configuration allows to change the load after calibration. By this method, different loads are connected to the NVD to evaluate the sensitivity of the NVD to load impedance mismatches and to make a comparison to other designs.

The nonlinear verification device is measured with an input RF (2 GHz) power of 10 dBm in order to drive it in nonlinear mode, and it is biased at 0.1 V.

To have a better estimate of the measured FOM, which is strongly load dependent, we did the measurements with 180 loads, unlike [5], [6] that used only five loads. We achieved 180 loads by changing the impedance at the fundamental frequency and second harmonic by a dual-frequency passive tuner (Fig. 6). We defined nine states for the reflection coefficients at the fundamental frequency $|\Gamma_{l,f0}|$= [0.05, 0.1, 0.2, 0.3, 0.4, 0.5, 0.6, 0.7, 0.8], two states for the angle at the fundamental frequency $\angle\Gamma_{l,f0}$=[0, 180], five states for the reflection coefficient at the second harmonic frequency $|\Gamma_{l,2f0}|$=$|\Gamma_{l,f0}|$ ×[0, 0.25, 0.5, 0.75, 1] and two states for the angle at the second harmonic frequency $\angle\Gamma_{l,2f0}$=[0, 180]. In fact, NVNA's port does not introduce a high reflection factor

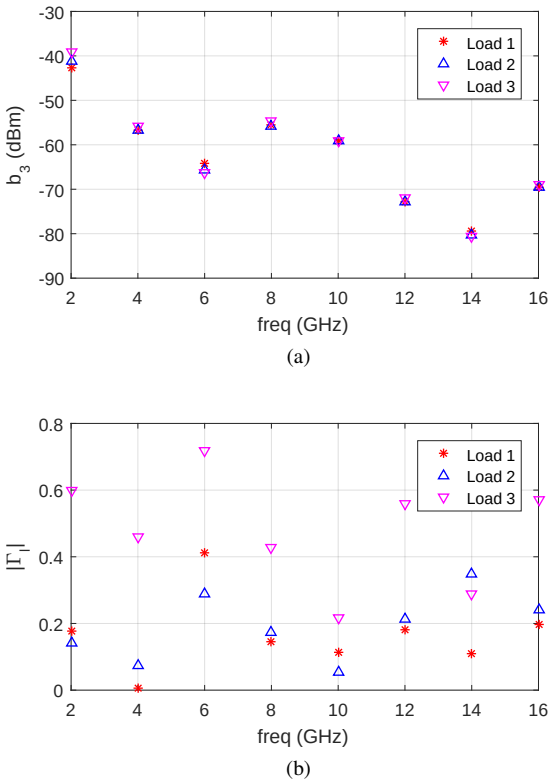

Figure 7. The NVD's response without mismatch correction 6 as the (a) output wave (b_3) for (b) three different loads.

such as $|\Gamma_l| = 0.8$, we decided to increase the mismatch by loadpull to evaluate the NVD's response under a severe condition that might happen by the user's mistake such as making a loose connection. The response of the NVD is changed as shown in Fig. 7a for three loads illustrated in Fig. 7b.

To plot any figures related to FOM and FOM_{nf0}, a variable Maximum Reflection Coefficient (MRC) is assumed. The loads that have $|\Gamma_{m,nf_0}|$ <MRC are considered in the calculation of FOM. Each time, the value of MRC is increased until all loads are included in the FOM calculation. The FOM_{nf0} per each of the harmonic frequencies (5) are shown in Fig. 8a. FOM_{nf0} results at higher frequencies, such as at 8 GHz and 10 GHz, are much better than the ones in [7]. Moreover, measurements are also performed at frequencies that have not

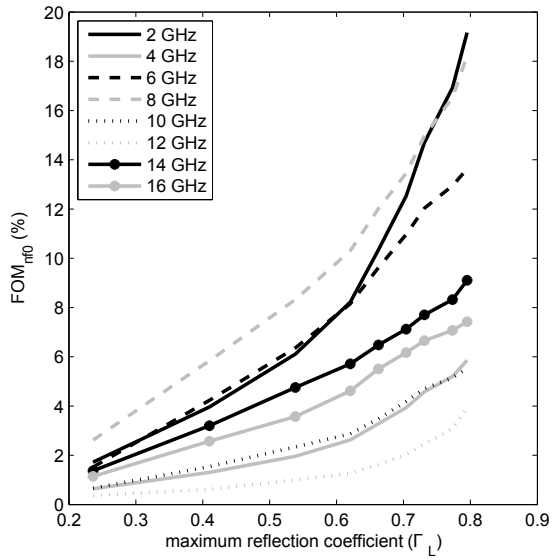

(a)

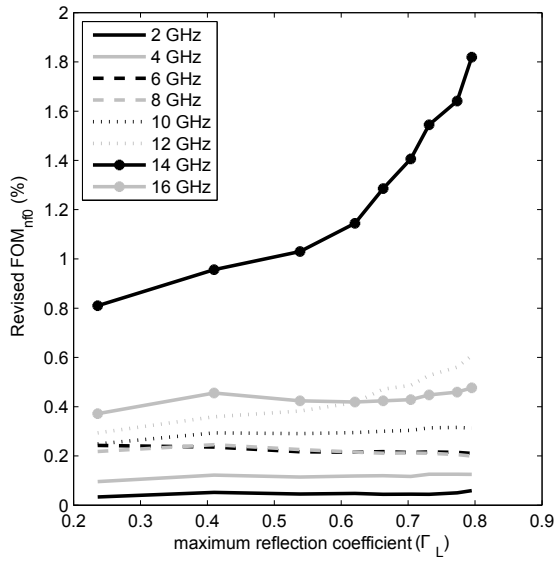

(b)

Figure 8. (a) FOM_{nf_0} (5) and (b) Revised FOM_{nf_0} using (6) by considering the loads over frequencies that have $|\Gamma|$ less and equal than certain maximum reflection coefficient among 180 loads (passive loadpull measurements).

been reported for other designs (12, 14 and 16 GHz), and the FOM_{nf_0} at those frequencies is low (less than 13%) even for high load impedances ($|\Gamma| < 0.8$). The FOM_{nf_0} can reach 40% for a design that is sensitive to mismatch, and it has considerable deviation at higher frequencies [7].

To compare this design to its amplifier-based counterpart [6], the FOM (4) is calculated based on the loads corresponding to $|\Gamma| < 0.5$, and the results are shown in Table I. The authors reported FOM for three input power levels (Table I). In the calculation of total FOM (4), we included all measured frequencies , i.e., from 2 GHz until 16 GHz (eight harmonic). Even though our design is simpler, the FOM results are

Table I
REPORTED FOM (4) FROM [5], [6] WITH VARIATION OF LOAD IMPEDANCE SATISFYING THE CONDITION ($|\Gamma_{m,nf_0}| < MRC$).

	Input power (dBm)	Amplifier	MRC	Freq (GHz)	(4) FOM (%)
[5]	-	Yes	0.2	2-10	1.5
[6]	10	Yes	0.5	2-14	7.7
This design	10	No	0.5	2-16	5.1

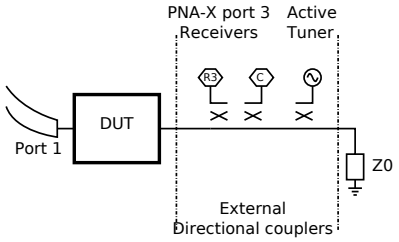

Figure 9. Measurement setup to change the load by active load-pull method using the second source of the NVNA (PNA-X).

similar to the amplifier based approach.

In addition, active load-pull measurements have been performed at each frequency, i.e., 2 GHz, 4 GHz, 6 GHz, and 8 GHz to evaluate the sensitivity of the response for each frequency while the impedance of other frequencies is fixed. The measurement setup is shown in Fig. 9. We defined eight states for the reflection coefficients at the desired frequency $|\Gamma_{l,nf0}|$= [0.1, 0.2, 0.3, 0.4, 0.5, 0.6, 0.7, 0.8, 0.9], and six states for the angle at the desired frequency $\angle\Gamma_{l,nf0}$=[-180:60:120]. The results are shown in Fig. 10. Regarding all active loadpull measurements performed at each frequency, i.e., 2 GHz, 4 GHz, 6 GHz, and 8 GHz, when the active loadpull measurement is performed at specific frequency, the corresponding FOM_{nf_0} is considerably changed while the FOM_{nf_0} at the other frequencies are almost kept constant and are less than 1%. This result confirms that the $FOM_{nf_0}$is not affected by $\Gamma_{kf_0}(k \neq n)$. This indicates that the influence of the loads on the NVD resembles a linear system. To check this conclusion, the variation Γ_{nvd,nf_0} is also evaluated.

Revised FOM: By applying the least squares fitting on a set of loads that have $|\Gamma_l|$ less than a certain value, $\hat{\Gamma}_{nvd,nf_0}$ can be estimated as we explained in Section II-B. We want to check how the $\hat{\Gamma}_{nvd,nf_0}$ is changed by increasing the load impedance mismatch.

We consider the first 20 loads (lower Γ_l) among 180 loads, and calculate the $\hat{\Gamma}_{nvd,nf_0}$. Then, we include 20 more loads in the set of loads which the least squares would be applied to. We repeat the procedure until we include all 180 loads. The results are shown in Fig. 11. This result indicates that the state of NVD is almost independent of the loads. Therefore, using (6) is valid in our case.

The correction (6) is used in (4) and (5) to have the revised FOM and the revised FOM_{nf_0}, respectively. This correction is done on the results of passive loadpull measurements. The revised format for FOM and FOM_{nf0} normalizes any phase

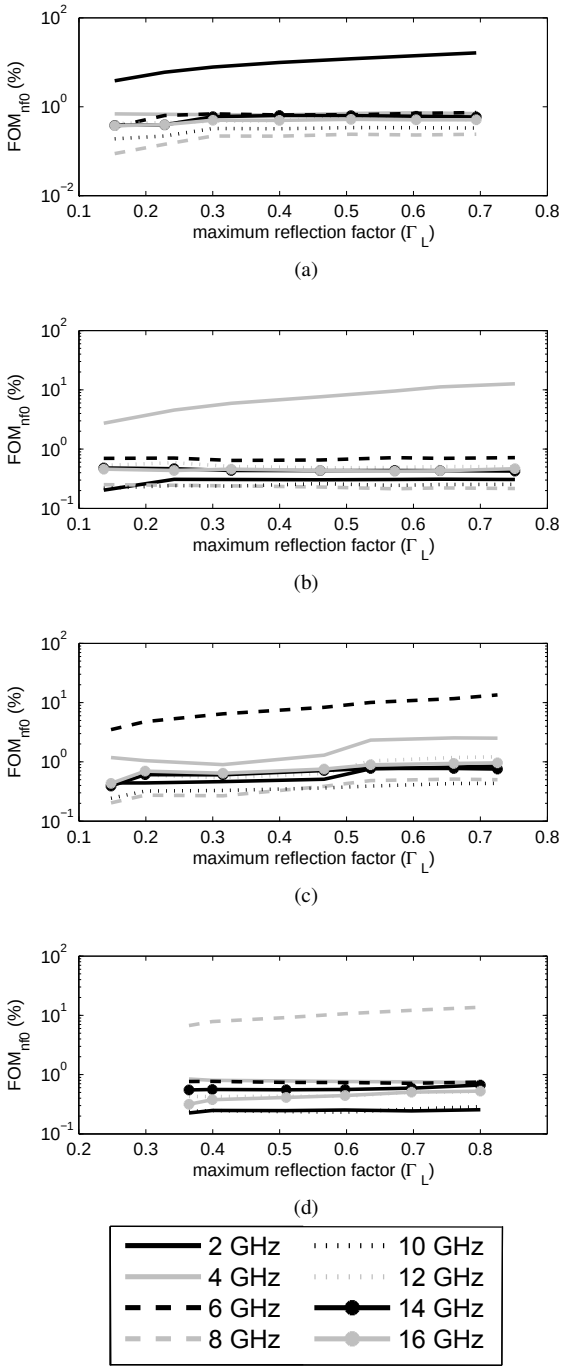

Figure 10. FOM_{nf_0} (5) by considering the loads over frequencies that have $|\Gamma|$ less and equal than certain maximum reflection coefficient among 48 loads. The legend is applicable to active loadpull at (a) 2 GHz, (b) 4 GHz, (c) 6 GHz, and (d) 8 GHz.

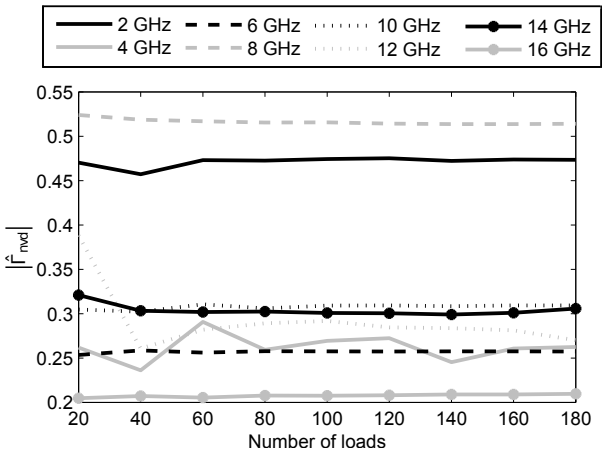

Figure 11. The calculated $\left|\hat{\Gamma}_{nvd,nf_0}\right|$ by considering different loads. The first 20 loads relates to the lowest mismatch. Each time, higher mismatch loads are included until all 180 loads are included.

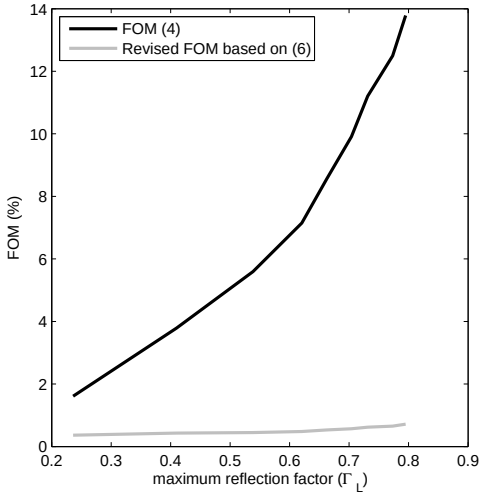

Figure 12. (a) FOM (4) and (b) Revised FOM using (6) by considering the loads over frequencies that have $|\Gamma|$ less and equal than certain maximum reflection coefficient among 180 loads.

variations first and corrects for the uplift of the b-wave due to load mismatch to give the underlying value of the b-wave. The revised FOM_{nf_0} at each frequency is shown in Fig. 8b. Comparing Fig. 8a and Fig. 8b signifies the overestimation of FOM compared to the revised FOM . The revised FOM_{nf_0} has an advantage to express that even by correction (6), the value of b_3-wave at 14 GHz and 16 GHz are not as load independent as other frequencies. This is also what we expected since the isolation of the output passive block at higher frequencies is not as good as at lower frequencies (Fig. 4).

Using the revised FOM_{nf0} indicates at which frequency the NVD's response is not consistent by varying the load. The revised FOM_{nf0} in Fig. 8b indicates the worst performance happens at 14 GHz that could be ascribed to the behavior of the output passive block, which shows S_{22} lower than S_{23} (Fig. 4).

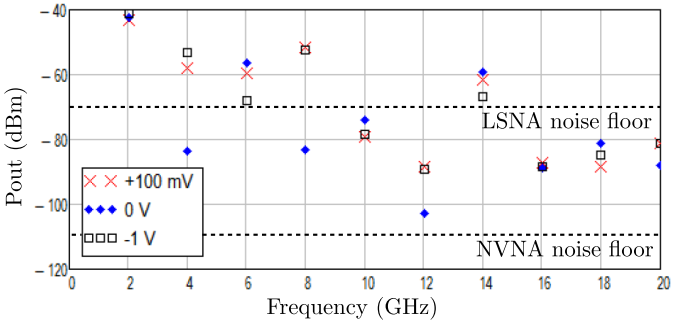

Figure 13. NVNA measurement of the output wave (b_3) for three different bias conditions.

By using (6) to calculate the revised FOM_{nf0}, the results become almost constant and independent of mismatch. The same phenomenon happens for the revised FOM, as shown in Fig. 12.

Bias Behavior

Altering the bias conditions for the diodes changes their characteristics, thereby changing the harmonic content as explained in Section II. For example, at 0 V bias the even harmonics are strongly suppressed (Fig. 13). Biasing the NVD in a desired way is essential for comparison between two different measurements. DC source's reliability is important. There is no problem, if the DC source has a good quality to provide the desired DC voltage. Otherwise, for positive bias the rate of change of static current is very high. A 10 mV error gives a noticeable change in the current. The simplest two-state configuration is 0 V (short) and self bias (open), differently from amplifier-based NVD which needs biasing. Using diode provides a feature to omit the dependency on DC source, but not biasing the NVD results in lower output power. This NVD is mainly designed for NVNA instrument. NVNA's noise floor with 30 Hz as IFBW is -114 dBm, therefore an instrument such as NVNA is capable of measuring low power output signal of the NVD. Using NVD for Large Signal Network Analyzer (LSNA) [2] is possible with conditions. The noise floor in LSNA with 10 MHz as IFBW and 12 KHz as resolution bandwidth is -70 dBm [23]. Not biasing the NVD limits the number of measurable harmonics to three. By having a reliable DC source measuring five harmonics is possible in LSNA configuration.

Stability Measurement

Stability, drift or aging evaluations are application dependent that might need months or 48 hours [9]. An NVNA should usually be re-calibrated and verified after two-three days. In normal operation, the NVD is used for a few minutes only at a time, and it is recommended to send the NVD back to an NMI to remeasure it after several usages. Therefore, in this application 84-hour measurement is sufficient. Aging and long-term effect is not in the scope of this paper, however measuring the NVD is still essential and should be done in future works to evaluate the aging changes rate of the NVD.

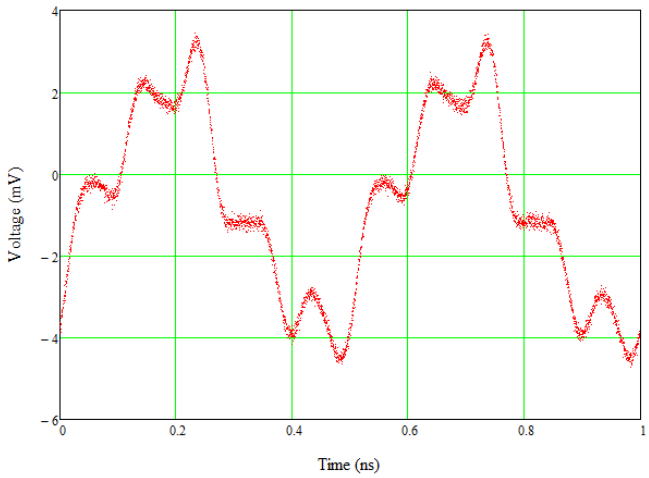

Figure 14. The output signal of the NVD measured by a DSO.

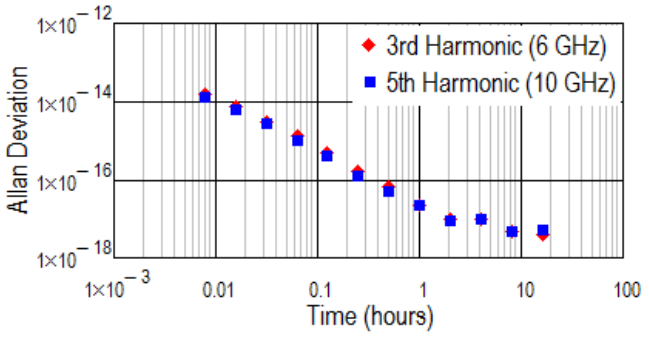

Figure 15. Allan Deviation analysis of the harmonic content (0 V bias).

The response of the NVD was measured over an 84-hour period by using a Digital Sampling Oscilloscope (DSO). An example of the measured time domain waveform is shown in Fig. 14. Because the focus of measurement is to evaluate the NVD stability, the NVD is biased at 0 V bias without using DC supply. The measurements were performed in a standard laboratory environment ($23 \pm 2°\mathrm{C}$) using a DSO and synthesizers to provide the stimulus and timebase correction [24]. In this measurement, the waveforms were averaged to reduce the noise since the signal-level is low. Fig. 15 shows the Allan deviation of the normalized b_3-wave (2). Measurements taken at 6 GHz and 10 GHz, third and fifth harmonic respectively, have only been used since the other components are noisier and therefore, estimation of Allen deviation would not converge. The largest signal components (fundamental and third harmonic) show a slight slope change at 2-4 hours of operation.

V. Conclusions

In this work, a verification device for nonlinear vectorial calibrations has been developed, and its stability, load-pull tolerance and behavior with bias have been evaluated. Passive load-pull measurements were performed to evaluate the FOM and make a comparison with other designs. The proposed

device, despite its simplicity, shows better performance with respect to its counterparts based on the existing FOM. However, the existing FOM has a problem, which was explained. To address this, we introduced a correction to the existing FOM definition. The revised FOM is validated by performing active load-pull measurements and subsequently checking the estimated Γ_{nvd} by considering different loads. The revised FOM is insensitive to the device output match and identifies its load-pull tolerance by excluding the contribution of load-pull variation distribution. The revised FOM_{nf_0} shows that the response of the NVD at frequencies 2 GHz till 12 GHz exhibit less changes to different loads than at other frequencies, which agrees with our expectation based on the S-parameters of the output passive block. The results show that the device is stable and shows good resilience to the impedance-match environment. This raises the possibility that the NVD element could potentially be included in an e-calibration system (ECU) as these devices also include temperature stabilization, which would further improve the NVD performance. Since this circuit is made of a diode, that is a relatively simple device, and transmission lines, as compared to other designs, evaluating the uncertainty of such a traceability path seems feasible.

REFERENCES

[1] P. Tasker, "Practical waveform engineering," *IEEE Microwave Magazine*, vol. 10, no. 7, pp. 65–76, Dec 2009.

[2] W. Van Moer and Y. Rolain, "A large-signal network analyzer: Why is it needed?" *IEEE Microwave Magazine*, vol. 7, no. 6, pp. 46–62, Dec 2006.

[3] G. Avolio, A. Raffo, J. Jargon, P. D. Hale, D. M. M. P. Schreurs, and D. F. Williams, "Evaluation of uncertainty in temporal waveforms of microwave transistors," *IEEE Transactions on Microwave Theory and Techniques*, vol. 63, no. 7, pp. 2353–2363, July 2015.

[4] A. Rumiantsev and N. Ridler, "VNA calibration," *IEEE Microwave Magazine*, vol. 9, no. 3, pp. 86–99, Jun 2008.

[5] H. Jang, Y. Ko, and P. Roblin, "Development of Multiharmonic Verification Artifact for the LSNA and NVNA (MTT-11)," *IEEE Microwave Magazine*, vol. 14, no. 1, pp. 134–139, Jan 2013.

[6] K. Wang, S. Adhikari, A. Ghiotto, and K. Wu, "Multiharmonic Generator for Large-Signal-Network-Analyzer Verification," *IEEE Microwave Magazine*, vol. 15, no. 1, pp. 120–128, Jan 2014.

[7] M. Rajabi, D. A. Humphreys, T. Nielsen, P. Barmuta, and D. Schreurs, "Design and analysis of a verification device for the nonlinear vector network analyzer," in *85th Microwave Measurement Conference (ARFTG)*, May 2015, pp. 1–4.

[8] N. Ridler, R. Clarke, M. Salter, and A. Wilson, "The Trace Is on Measurements: Developing Traceability for S-parameters Measurements at Millimeter and Submillimeter Wavelengths," *IEEE Microwave Magazine*, vol. 14, no. 7, pp. 67–74, Nov 2013.

[9] D. F. Williams, K. A. Remley, J. M. Gering, G. S. Lyons, C. Lineberry, and G. S. Aivazian, "Comparison of Large-Signal-Network-Analyzer Calibrations," *IEEE Microwave and Wireless Components Letters*, vol. 20, no. 2, pp. 118–120, Feb 2010.

[10] P. Barmuta, D. Ribeiro, K. Wang, G. Avolio, M. Rajabi, A. Lewandowski, G. P. Gibiino, J. Szatkowski, D. Schreurs, P. Hale, K. Remley, and D. Williams, "Comparing lsna calibrations: Large-signal network analyzer round robin," *IEEE Microwave Magazine*, vol. 17, no. 2, pp. 59–64, Feb 2016.

[11] D. A. Humphreys, M. Rajabi, D. Schreurs, and T. Nielsen, "A nonlinear verification device for nonlinear vector network analyzers," in *Conference on Precision Electromagnetic Measurements (CPEM)*, July 2016, pp. 1–2.

[12] J. Verspecht and D. E. Root, "Polyharmonic Distortion Modeling," *IEEE Microwave Magazine*, vol. 7, no. 3, pp. 44–57, Jun 2006.

[13] Y. Rolain, W. Van Moer, C. Gaquière, D. Ducateau, M. Fernandez Barciela, D. Schreurs, M. Vanden Bossche, and F. Verbeyst, "A round-robin benchmark for the Large Signal Network Analyzer," in *26th Benelux Meeting on Systems and Control*, Lommel, Belgium, Mar 2007, p. 82.

[14] G. Paillonc y and M. Vanden Bossche, "Gaining advanced insight in the phase stability of comb generators using a Large-Signal Network Analyzer," in *IEEE/MTT-S International Microwave Symposium*, Jun 2007, pp. 1193–1196.

[15] J. Jargon, D. DeGroot, and D. Vecchia, "Repeatability study of commercial harmonic phase standards measured by a nonlinear vector network analyzer," in *62nd Microwave Measurements Conference (ARFTG)*, 2003, pp. 243–258.

[16] J. Stenarson, C. Eio, and K. Yhland, "A calibration procedure for electronic calibration units," in *84th Microwave Measurement Conference (ARFTG)*, Dec 2014, pp. 1–6.

[17] M. Golio and J. Golio, *RF and Microwave Circuits, Measurements, and Modeling: Rf and Microwave Handbook*, 2nd ed. Boca Raton, FL, USA: CRC Press, Inc., 2007.

[18] D. Humphreys and A. Gifford, "Novel microwave reflectometer for accurate characterisation of high-speed photodiode optoelectronic response," *Electronics Letters*, vol. 28, no. 23, pp. 2138–2140, Nov 1992.

[19] S. Adhikari, A. Ghiotto, K. Wang, and K. Wu, "Development of a Large-Signal-Network-Analyzer Round-Robin Artifact," *IEEE Microwave Magazine*, vol. 14, no. 1, pp. 140–145, Jan 2013.

[20] E. R. Ehlers, S. W. Johnsen, and D. A. Gray, "Extending Millimiter-Wave Diode Operation to 110 GHz," *Hewlett-Packard Journal*, vol. 37, no. 11, pp. 10–14, Nov 1986.

[21] Y. Zhang and M. Lin, "An NVNA poly-harmonic inter-modulation phase reference based on SRD comb generator and multi-tone stimulus," in *Conference on Precision Electromagnetic Measurements (CPEM)*, Jul 2012, pp. 108–109.

[22] D. A. Humphreys, M. Hudlicka, and I. Fatadin, "Calibration of wide-band digital real-time oscilloscopes," in *29th Conference on Precision Electromagnetic Measurements (CPEM)*, Aug 2014, pp. 698–699.

[23] S. J. Doo, P. Roblin, S. Lee, D. Chaillot, and M. V. Bossche, "Pulsed-IV pulsed-RF measurements using a large signal network analyzer," in *65th ARFTG Conference Digest*, June 2005.

[24] D. A. Humphreys and F. Bernard, "Compensation of sampling oscilloscope trigger jitter by an In-phase and quadrature referencing technique," in *ARMMS Conf.*, Abbingdon, UK, 18-19 Apr 2005, pp. 1–8.

Mohammad Rajabi was born in Esfahan, Iran. He received the master's degree in electronics and information technology (with honors) from Vrije Universiteit Brussel (VUB), Brussels, Belgium, in 2013. He is currently working toward the Ph.D. degree at KU Leuven, Leuven, Belgium.

He has been with the Departement Elektrotechniek-ESAT, TELEMIC division, KU Leuven since 2013. His research interests include RF circuit design, measurement, and modeling of high-frequency measurement equipment. His current research is Simultaneous Wireless Information and Power Transfer (SWIPT).

David A. Humphreys was born in Epsom, UK in 1956. He received a BSc in electronic engineering from Southampton University, UK in 1978 and a PhD in electronic engineering from London University, UK in 1990. His thesis concerned the accurate measurement of high-speed optoelectronic devices at telecommunication wavelengths. He joined the National Physical Laboratory, Teddington, UK in 1978 developed metrology for photodiodes at up to mm-wave frequencies, optical wavelength capabilities for optical communications and waveform metrology for RF communications. His recent interests include full-waveform characterization of the primary-standard electro-optic sampling system, RF waveforms for wireless communications, EVM, 5G, nonlinear RF measurements and correlated waveform uncertainties. He was the coordinator for the EMRP IND51 "Metrology for RF and Optical Communications" joint research project from June 2013 until June 2016. He is Vice-Chair of the P1765 IEEE pre-standards group on "The uncertainties in Error-Vector-Measurement (EVM)".

Dr. Humphreys is a Chartered Engineer and a Fellow of the IET (UK) and a Research Fellow at the University of Bristol, UK. He was awarded the IEE Ambrose Fleming Premium in 1987 and has published over 95 peer reviewed journal and conference papers.

Gustavo Avolio (M'12) was born in Cosenza, Italy, in 1982. He received the M.Sc. degree in electronic engineering from the University of Calabria, Cosenza, in 2006, and the Ph.D. degree in electronic engineering from the Katholieke Universiteit Leuven, Leuven, Belgium. He is currently a Post-Doctoral Researcher supported by FWO Vlaanderen, Belgium. In 2013 and 2014, he has been a Visiting Scientist with the National Institute of Standards and Technology, Boulder, CO, USA. Since 2009, he has often been a Visiting Scientist with the University of Ferrara, Ferrara, Italy. His current research interests include large-signal measurements and nonlinear modeling of advanced microwave devices.

Paweł Barmuta obtained the dual Ph.D. degree (with honors) in electronic engineering from Warsaw University of Technology, Warsaw, Poland and KU Leuven, Leuven, Belgium, in 2016. He is currently an Assistant Professor at the Department of Electronics and Information Technology, Warsaw University of Technology, and also a Research Associate with KU Leuven. His research interests are nonlinear microwave measurements, experiment design, calibration techniques, and microwave measurements in microbiology.

Konstanty R. Łukasik (S'17) was born in Poland in 1990. He received the BSc and the MSc degrees in electrical engineering from Warsaw University of Technology in 2014 and 2015, respectively. At the International Microwave Conference MIKON 2016 (Cracow, Poland), Mr. Łukasik was a recipient of the third prize of AP/AES/MTT Joint Chapter of the IEEE Poland Section for the best master thesis. Now he is pursuing a dual-degree PhD at KU Leuven and Warsaw University of Technology. His current research interests include microwave measurements, design of experiments, and measurement uncertainty analysis.

Troels S. Nielsen received the Master and Ph.D. degrees in electrical and electronic engineering from Aalborg University, Denmark in 2002 and 2006, respectively. He is currently a Research Scientist with the Measurement Research Labs. in Keysight Technologies, Rotselaar, Belgium. From 2005 to 2009, he worked as Senior RF Design Engineer in the Corporate R&D Modeling Group in RFMD, Greensboro, North Carolina, USA. His current work focuses on research and development of large-signal nonlinear models for III-V Technology power amplifiers and large-signal measurements for nonlinear model development and validation. His technical interests include techniques for system level modeling, nonlinear system identification techniques, large-signal nonlinear measurements, and power amplifier linearization techniques. He has authored a dozen technical papers, articles, and book contributions within the fields of RF/microwave IC design, characterization, and modeling.

Dominique M. M.-P. Schreurs (S'90–M'97–SM'02–Fellow) received the M.Sc. degree in electronic engineering and Ph.D. degree from the University of Leuven (KU Leuven), Belgium. She is now a Full Professor with KU Leuven. She has been a Visiting Scientist with Agilent Technologies, ETH Zurich, and the National Institute of Standards and Technology (NIST). Her main research interests concern the microwave and millimetre wave characterization and modeling of active devices and bioliquids, as well as system design for wireless telecommunications and biomedical applications. Prof. Schreurs is serving on the AdCom of the MTT Society. She is an IEEE Fellow, Chair of MTT-S Meetings & Symposia Committee, past MTT-S Distinguished Microwave Lecturer, and past Editor-in-Chief of IEEE Trans. Microwave Theory and Techniques. She serves as Vice-President on the Executive Committee of the ARFTG organization, and is general chair of the 2007, 2012, and 2018 Spring ARFTG Conference. Prof. Schreurs was co-chair of the European Microwave Conference (EuMC) in 2008.